Factors Controlling Upper-Troposphere Water Vapor

YONG ZHU AND REGINALD E. NEWELL

Department of Earth, Atmospheric and Planetary Sciences, Massachusetts Institute of Technology, Cambridge, Massachusetts

WILLIAM G. READ

Jet Propulsion Laboratory, California Institute of Technology, Pasadena, California

(Manuscript received 8 September 1998, in final form 8 May 1999)

ABSTRACT

The seasonal changes of the upper-tropospheric humidity are studied with the water vapor data from the Microwave Limb Sounder on the National Aeronautics and Space Administration's *Upper Atmosphere Research Satellite*, and the winds and vertical velocity data obtained from the European Centre for Medium-Range Weather Forecasts. Using the same algorithm for vertical transport as that used for horizontal transport (by Zhu and Newell), the authors find that the moisture in the tropical upper troposphere may be increased mainly by intensified local convection in a small portion, less than 10%, of the whole area between 40°S and 40°N. The contribution of large-scale background circulations and divergence of horizontal transport is relatively small in these regions. These dynamic processes cannot be revealed by the traditional analyses of moisture fluxes. The negative response suggested by Lindzen, with enhanced convection in the Tropics being accompanied by subsidence drying in the subtropics, also exists, but the latter does not apparently dominate in the moisture budget.

1. Introduction

The effect of increasing sea surface temperature (SST) on the change of moisture in the upper troposphere has received wide interest, since the hypothesis of a possible negative response was proposed by Lindzen (1990). This hypothesis was detailed by Sun and Lindzen (1993). They argued that the cumulus-induced time and zonal mean large-scale subsidence could be increased if sea surface temperatures increased, while the contribution of eddy fluxes would be negligible. According to Rasmusson (1972) and Peixoto and Oort (1992), the tropical water vapor transport by time and zonal mean flows is dominant only below 500 hPa; the fluxes carried by stationary eddies and transient perturbations may be greater in the upper troposphere although hitherto there have been few direct observations there. A general circulation model used by Allam and Tuck (1984) showed that the meridional mass fluxes in the upper troposphere were dominated by the time and zonal mean flows at all latitudes, while the moisture flux carried out by transient and stationary eddies were comparable with the flux contributed by the time and zonal mean flows, except in the tropical regions. Del Genio et al. (1994) reported that the upper-tropospheric moisture response in their general circulation model is positive, since the drying by the mean Hadley cell subsidence was offset by the moistening resulting from convergence of the vertical eddy flux. Cess et el. (1990) also found that some general circulation models yielded a positive response of upper-troposphere humidity (UTH) from increasing SST. On the other hand, Chou (1994) and Fu et al. (1997) argued that enhanced tropical convection reduced the UTH in the adjacent subtropical areas, shown by data analyses and model results. These consequences appear to be in conflict with each other, but both may be right. At this point, then, the published empirical analyses and model results do not consistently yield the same sign for the relation between increasing SST and UTH.

The Microwave Limb Sounder (MLS) on the National Aeronautics and Space Administration (NASA) *Upper Atmosphere Research Satellite* (*UARS*) provided unique satellite datasets of UTH, which include measurements in the presence of cirrus (Read et al. 1995). A new version of the humidity data (V490) is now available at four pressure levels: 464, 316, 215, and 147 hPa, based on the relative humidity with respect to ice. The data coverage is continuous from 34°S to 34°N, with a change every 36 days between 34°–80°N and 34°–80°S. A discussion of the new data and comparisons with other datasets has been given by Sandor et al. (1998). An amplification of this discussion concerns the fact that

Corresponding author address: Yong Zhu, Department of Earth, Atmospheric and Planetary Sciences, MIT, 54-1822, 77 Massachusetts Avenue, Cambridge, MA 02139.

© 2000 American Meteorological Society

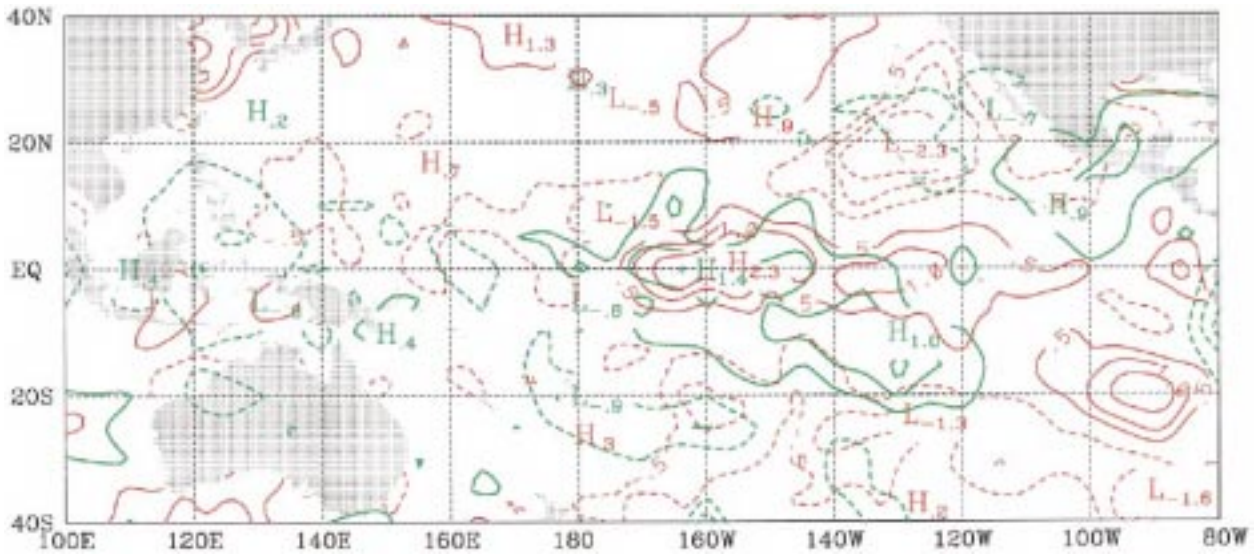

FIG. 1. The differences of one-season climatologies. Red contours depict the seasonal mean SST in Dec 1991–Feb 1992 minus that in Dec 1993–Feb 1994; units: C°. The difference of MLS water vapor column content within 316–147 hPa is in green; units: 0.1 kg m^{-2}.

MLS is sensitive to ice emission but unlike Stratospheric Aerosol and Gas Experiment II (SAGE-II), the emission cross section of ice is half that of vapor (Read et al. 1995); therefore, observations can be made in its presence. Nonscattering emission from typical amounts of thin cirrus (3 mg m^{-3}) and subvisible cirrus (K3 mg m^{-3}) would be expected to cause an overestimation of UTH not more than 6% (for 3 mg m^{-3}), which is probably unimportant because this is quite less than the systematic UTH measurement error (typically 10%–20%). Typical particle sizes in thin cirrus are below the scattering threshold and are not expected to have a significant scattering contribution. Thick cirrus from convection can cause large signal enhancement due to scattering upwelling radiation and high density ice emission, and this has been observed in the data. Generally, it is assumed that cirrus exists in saturated air and the retrieved values are trimmed to be the smaller of the measured or 100% relative humidity as a way of minimizing vapor errors due to ice contamination. Another step taken to minimize sampling problems was as follows. For the four 1991–92 seasons 330 days were well sampled and for 1992–93 317 days were well sampled, while for 1993–94, 272 days were sampled with three months being 16 or less and 6 months less than 19 days. To avoid a potential sampling problem, we confined the analyses to the first two years. For each of the 647 days used in our analysis an objective computer analyzed map has been drawn of water vapor mixing ratio for each of the four levels 464, 316, 215, and 147 hPa. Each map has been inspected individually and for any dates that showed potential problems, all the levels for that date have been rejected. This step reduced the data sample by about 2% but improved its fidelity.

We will use the MLS humidity data together with the European Centre for Medium-Range Weather Forecasts (ECMWF) winds and vertical velocity to study the seasonal variations of UTH and the related dynamic mechanisms.

Section 2 comments further on the sign of the response and examines it from the MLS data; section 3 presents meridional and vertical fluxes of water vapor; section 4 investigates seasonal changes of UTH insofar as they may represent the response to surface heating; section 5 discusses the dynamical processes governing both positive and negative responses of UTH; section 6 emphasizes the role of slantwise convection; and section 7 discusses the conclusions.

2. Positive or negative response?

Figure 1 compares the differences of SST and MLS UTH between an El Niño season in 1992 and a pre–La Niña season in 1994. In the tropical Pacific, the ocean surface was generally colder over the western part, but warmer over the eastern part in early 1992. Two areas of negative SST difference occurred also on both sides of the warm pool. A similar pattern is found also in the difference of MLS UTH. This feature suggests a positive correlation between the UTH and local SST, as reported with different datasets by others (Raval and Ramanathan 1989; Rind et al. 1990; Soden and Fu 1995). Now, if we compare the low MLS UTH over the eastern subtropical Pacific with the warm tropical ocean water beneath, a negative correlation results. Certainly, the negative correlation does not mean that the local correlation between UTH and SST was also negative. Higher UTH in one region is often connected with deep convection

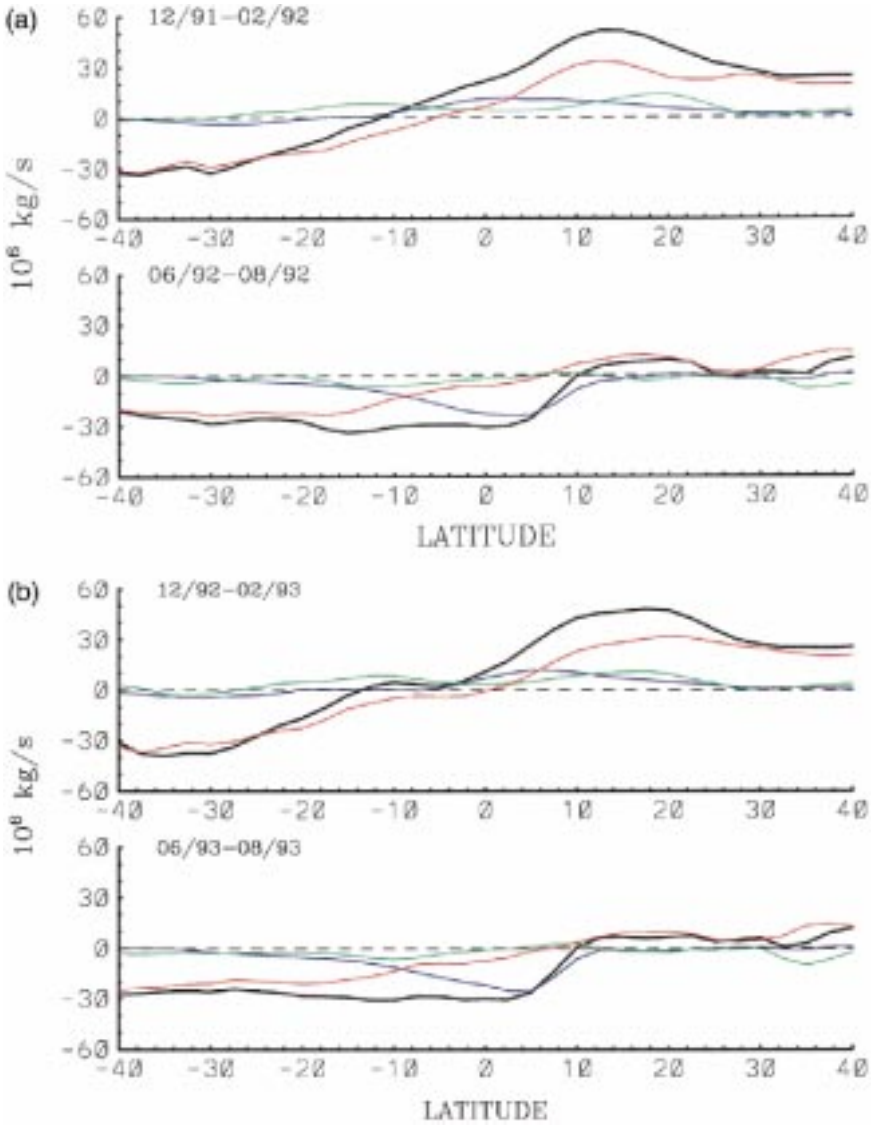

FIG. 2. MLS UTH fluxes by ECMWF winds; blue: time and zonal mean flow fluxes, green: stationary eddy fluxes, red: transient perturbation fluxes, and black heavy: the total mean fluxes.

in a region far removed as seen in an example we provided elsewhere (Newell et al. 1997, Fig. 5). This gives a limitation on the study of the greenhouse effect in terms of the response of UTH in the tropical El Niño events. While the high relative humidities (>80%) in Fig. 1 spanning the latitudes from about 20°N to 20°S are based on ECMWF analysis, they were verified by the presence of cirrus observed by airborne lidar from the intertropical convergence zone at about 10°S to north of Guam at 14°N (Newell et al. 1996). One particular general circulation model, which produced the negative response of subtropical UTH to the intensified deep convection during the 1987 El Niño (Fu 1997), could also produce positive response to an increase of SST (Cess et al. 1990).

3. UTH fluxes by ECMWF winds

The time and zonal mean meridional fluxes of water vapor may be partitioned into (Rasmusson 1972)

$$(\overline{vq}) = (\overline{v})(\overline{q}) + (\overline{v}^*\overline{q}^*) + (\overline{v'q'}), \qquad (1)$$

where v is the meridional wind component, and $q = \rho_w/\rho_a$ is the specific humidity (ρ_a and ρ_w represent the densities of air and water vapor, respectively). Analogously, the vertical fluxes may be written as

$$-\frac{1}{g}(\overline{wq}) = -\frac{1}{g}[(\overline{w})(\overline{q}) + (\overline{w}^*\overline{q}^*) + (\overline{w}'\overline{q}')] \qquad (2)$$

in the pressure coordinates, where $w = dp/(dt)$ and g is the gravitational acceleration. The three terms on the

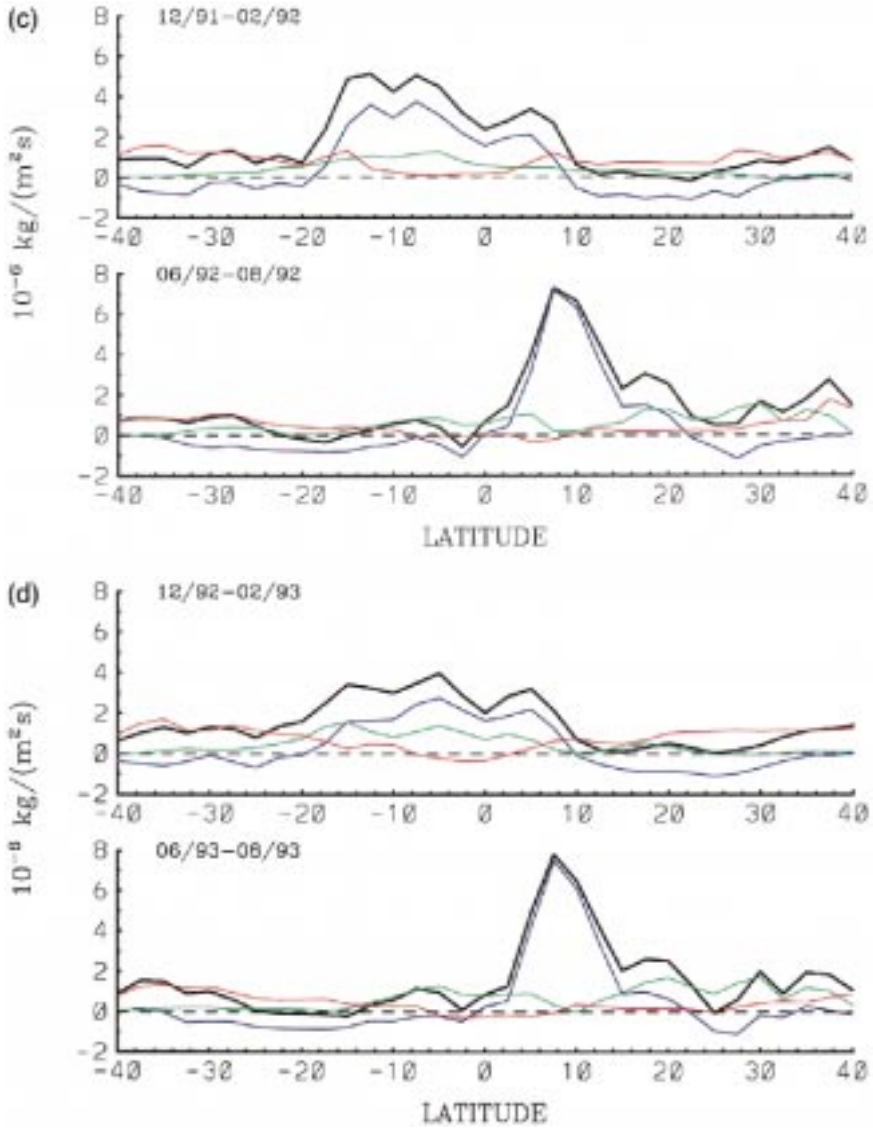

FIG. 2. (*Continued*) (a) Northward fluxes integrated from 464 to 147 hPa for 1991–92, (b) the same as (a) but for 1992–93, (c) upward fluxes on 464 hPa for 1991–92, and (d) the same as (c) but for 1992–93.

right-hand sides of the two equations are then called, respectively, the fluxes by the zonal mean flow, stationary eddies, and transient perturbations. The temporal mean is denoted by an overbar; the zonal mean is put in the square brackets, and the prime and asterisk indicate the deviations from the temporal and zonal means, respectively. Figure 2 gives the zonal distributions of the seasonal mean meridional and vertical MLS water vapor fluxes carried by ECMWF winds and vertical velocity in 1992 and 1993. The meridional fluxes are integrated from 464 to 147 hPa, for example,

$$Q_\phi = \frac{2\pi a}{g} \int_{147\,\mathrm{hPa}}^{464\,\mathrm{hPa}} (\overline{v}\overline{q}) \cos\phi \, dp, \qquad (3)$$

where a is the earth's radius and ϕ is latitude. The vertical fluxes are evaluated on 464 hPa. To use the same units as that of the meridional flux, (2) may be integrated to give

$$Q_w = \frac{-2\pi a^2}{g} \int_{\phi_1}^{\phi_2} (\overline{wq}) \cos\phi \, d\phi. \qquad (4)$$

Figure 2 shows that the meridional flux by the zonal mean flow was strongest in the tropical region, which transports moisture across the equator from the summer hemisphere to the winter hemisphere. In the northern summer, there was a mean southward flux over the equator. In the subtropical regions from 20° to 40°S the mean flow transports moisture poleward, except in the summer Northern Hemisphere. The total transport was poleward, showing divergence from about 10°S latitude, and dom-

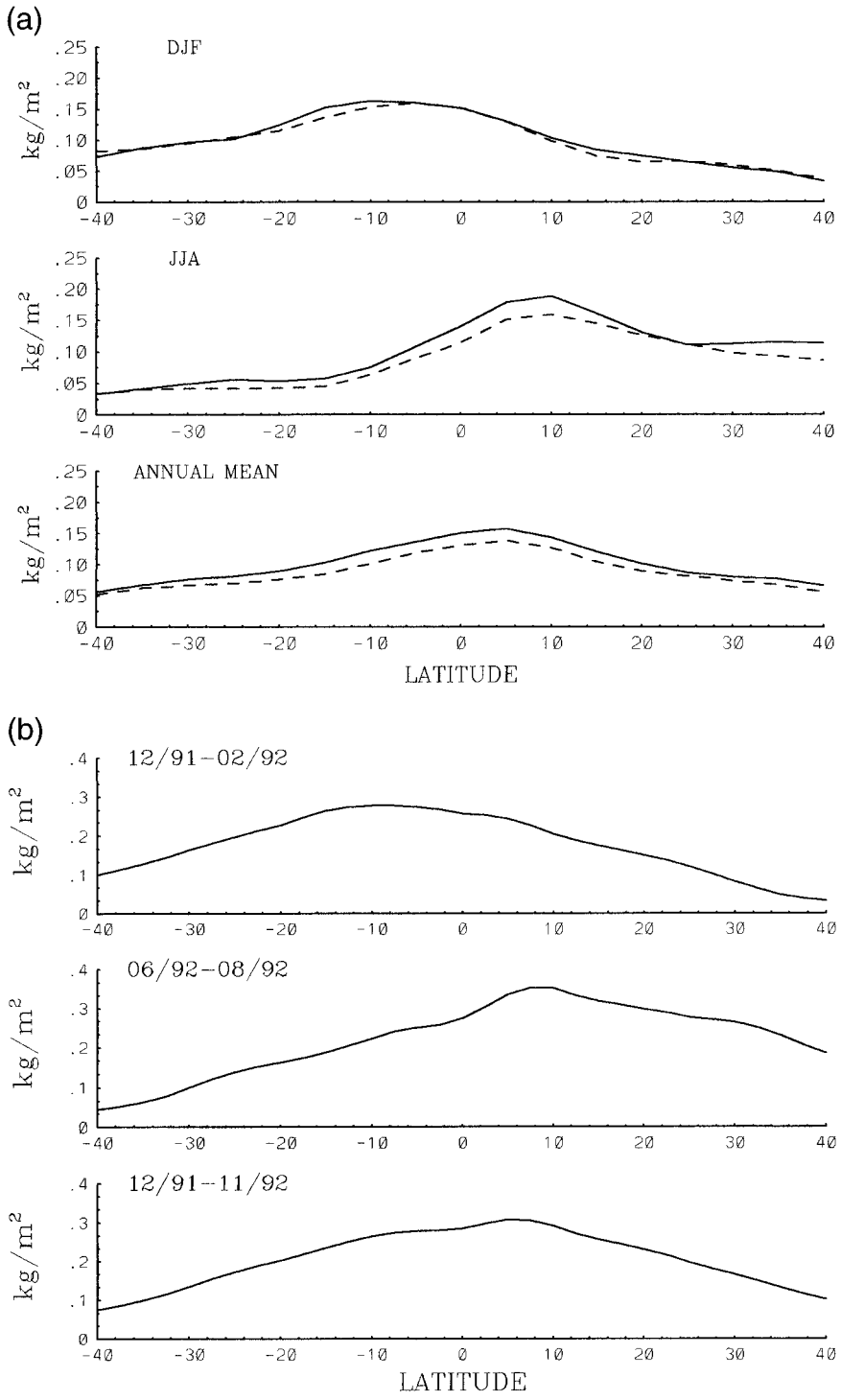

FIG. 3. (a) MLS water vapor column content in 316–147 hPa (solid: 1991–92, dashed: 1993–94), and (b) ECMWF water vapor column content in 300–150 hPa.

inated by transient perturbations in the subtropical regions. The stationary eddy flux was comparable with the mean flow flux in magnitude except near the equator. It was generally northward in northern winter but southward in northern summer. This implies that the seasonal phase changes in the stationary wind perturbations may not be correlated to the seasonal changes of humidity field.

The patterns for 1993 (Fig. 2b) are quite similar to those for 1992 (Fig. 2a), with both showing smallest

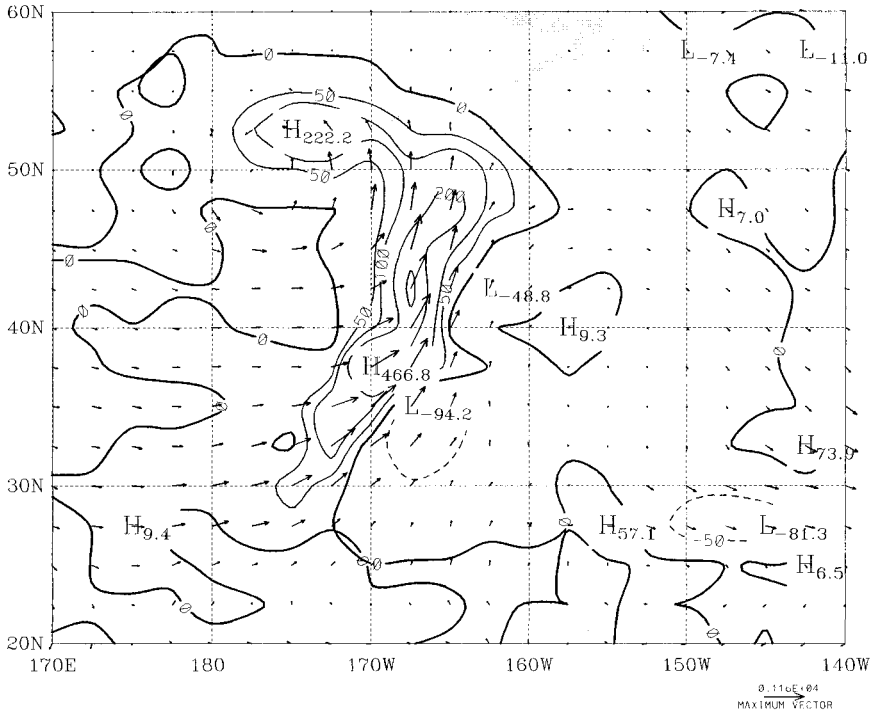

FIG. 4. Upward fluxes of water vapor on 500 hPa over a tropospheric river in units 10^{-6} kg m^{-2} s^{-1}, evaluated from ECMWF data at 1200 UTC 4 Jan 1992. The vectors represent the horizontal vapor fluxes integrated from 1000 to 300 hPa in units where the maximum vector is 1160 kg m^{-1} s^{-1}.

poleward fluxes in the Northern Hemisphere summer. In that season the water vapor flux divergence from 10°N is composed of a small transient eddy flux northward and a mean flow component southward into the Southern Hemisphere.

The ascending branch of the mean Hadley cell produced the largest upward water vapor flux in the middle troposphere (the blue curves of Figs. 2c,d), while the mean descending branch carried the moisture downward. The transient perturbations (the red curves) and stationary eddies (the green curves) pushed water vapor upward (i.e., downgradient in the humidity field) at almost all latitudes. The amount of eddy transport in the subtropical regions gives the same patterns with the tropical upward fluxes being higher in December 1991–February 1992, associated with El Niño in the tropical region.

4. Seasonal changes in UTH

The seasonal changes of UTH may give an example of the response to the surface heating. Figure 3a shows the MLS water vapor column content in the layer from 316 to 147 hPa. The values may be underestimated in the Tropics, as the mixing ratios may be lower than the balloon sonde data on 464 and 316 hPa when the vertical column is very moist (Sandor et al. 1998). However, the displayed layer seems remarkably wetter than the layer of 300–100 hPa measured from SAGE-II and analyzed by Chiou et al. (1997). The maximum content was found over the summer tropical areas around 10° latitude. The moisture over the subtropical regions increased nearly 100% from winter to summer in both hemispheres. This was unlikely to be produced by the interhemispheric transport, as the fluxes at the equator were toward to the winter hemisphere (Figs. 2a,b). Hence the seasonal change per se would argue for a positive response to additional surface heating.

The water column content from 300 to 150 hPa plotted from ECMWF data is displayed in Fig. 3b. The ECMWF humidity was systematically higher than that of MLS in the upper troposphere, while the patterns were similar. The differences could be produced by the errors either in ECMWF data or in *UARS* data. Usually the strong filamentary moisture flux as depicted in Fig. 4 (to be discussed below) presents the zone of high moisture concentration associated with strong surface convergence. The MLS water vapor may be underestimated over the regions of abundant moisture, by missing the peak values in the filamentary moist zones. This can be seen by comparing the daily moisture maps plotted using MLS and ECMWF data, respectively (figures are not shown). Read et al. (1999, personal communication) reported also that the MLS water vapor value is underestimated relative to radiosonde data by a larger factor at the higher values at 316 and 464 hPa, though

TABLE 1. Convective and background upward MLS water vapor fluxes, across 464 hPa (upper) for 1991–92, and (middle) for 1992–93; (lower) shows the vertical fluxes across 316 hPa for 1991–92. The numbers in parentheses are the convective fluxes within 20°S–20°N.

Convective F_z Background F_z 10^6 kg s^{-1}	40°–20°S	20°S–0°	0°–20°N	20°–40°N
Dec 1991–Feb 1992		**(424)**		
	111	313	111	56
	−39	*25*	*12*	**−12**
Mar 1992–May 1992		**(383)**		
	92	207	176	76
	−16	*10*	*12*	**−21**
Jun 1992–Aug 1992		(280)		
	41	34	**246**	96
	6	**−19**	*90*	*9*
Sep 1992–Nov 1992		(297)		
	73	93	**204**	70
	9	**−24**	*80*	**−15**
Annual mean		**(346)**		
	80	162	184	75
	−10	*−2*	*49*	**−10**
Dec 1992–Feb 1993		(318)		
	83	226	92	50
	5	*39*	*26*	*−3*
Mar 1992–May 1993		(284)		
	70	162	122	54
	4	*22*	*45*	*−8*
Jun 1993–Aug 1993		(311)		
	50	55	**256**	92
	5	**−21**	*82*	*6*
Sep 1993–Nov 1993		(364)		
	58	98	**266**	67
	9	**−55**	*49*	**−14**
Annual mean		(319)		
	65	135	**184**	66
	6	**−4**	*50*	**−5**
Dec 1991–Feb 1992		**(62)**		
	13	**46**	16	6
	−9	*2*	**−3**	**−2**
Mar 1992–May 1992		**(55)**		
	12	30	25	11
	−5	*−1*	*2*	**−3**
Jun 1992–Aug 1992		(44)		
	5	4	**40**	18
	1	**−6**	*12*	**−1**
Sep 1992–Nov 1992		(42)		
	10	12	**30**	8
	1	**−6**	*9*	**−4**
Annual mean		**(51)**		
	10	23	**28**	11
	−3	**−3**	*5*	**−3**

TABLE 2. Meridional and vertical influxes of MLS water vapor into the layer from 464 to 150 hPa for (upper) 1991–92 and (middle) 1992–93; (lower) from 316 hPa to 150 hPa for 1991–92. The numbers in parentheses are the net influxes. The annual mean in fluxes is converted into equivalent precipitation down from 464 hPa in (a) and (b), but from 316 hPa in (c).

Influx of F_y Influx of F_z 10^6 kg s^{-1}	40°–20°S	20°S–0°	0°–20°N	20°–40°N
Dec 1991–Feb 1992	−16	−38	−21	18
	72	**338**	*123*	*44*
Net influxes	(56)	(**300**)	(102)	(62)
Mar 1992–May 1992	−7	−36	−28	3
	76	*217*	*188*	*55*
Net influxes	(69)	(181)	(160)	(58)
Jun 1992–Aug 1992	6	4	−40	−1
	47	*15*	**336**	**105**
Net influxes	(53)	(19)	(**296**)	(**104**)
Sep 1992–Nov 1992	−9	−6	−45	−3
	82	*69*	*284*	*55*
Net influxes	(**73**)	(63)	(239)	(52)
Annual mean	−6	−19	−34	4
	70	*160*	*233*	*65*
Net influxes	(63)	(141)	(199)	(69)
P_e (mm yr^{-1})	(26)	(51)	(72)	(29)
Dec 1992–Feb 1993	−14	−27	−37	22
	88	**265**	*118*	*47*
Net influxes	(**74**)	(**238**)	(81)	(69)
Mar 1993–May 1993	−12	−34	−28	14
	74	*184*	*167*	*46*
Net influxes	(62)	(150)	(139)	(60)
Jun 1993–Aug 1993	1	2	−37	−5
	55	*34*	**338**	**98**
Net influxes	(56)	(36)	(**301**)	(**93**)
Sep 1993–Nov 1993	−17	−8	−49	5
	67	*43*	*315*	*53*
Net influxes	(50)	(35)	(266)	(58)
Annual mean	−11	−17	−37	9
	71	*131*	*234*	*61*
Net influxes	(60)	(114)	(197)	(70)
P_e (mm yr^{-1})	(28)	(49)	(84)	(24)
Dec 1991–Feb 1992	1	−17	3	7
	4	**48**	*13*	*4*
Net influxes	(5)	(**31**)	(16)	(11)
Mar 1992–May 1992	2	−10	−6	4
	7	*29*	*27*	*8*
Net influxes	(9)	(19)	(21)	(12)
Jun 1992–Aug 1992	2	11	−15	0
	6	*−2*	**52**	**16**
Net influxes	(8)	(9)	(**37**)	(**16**)
Sep 1992–Nov 1992	0	4	−13	1
	11	*6*	*39*	*4*
Net influxes	(**11**)	(10)	(26)	(5)
Annual mean	1	−3	−8	3
	7	*20*	*33*	*8*
Net influxes	(8)	(17)	(25)	(11)
P_e (mm yr^{-1})	(3)	(6)	(9)	(4)

the differences may not yet be well enough established to claim that this is the only reason for the contributed difference from the ECMWF data. It is noted that the water vapor balance depends not only on the large-scale circulations, but also on the microscale physics related to the surface water evaporation, water vapor condensation and precipitation.

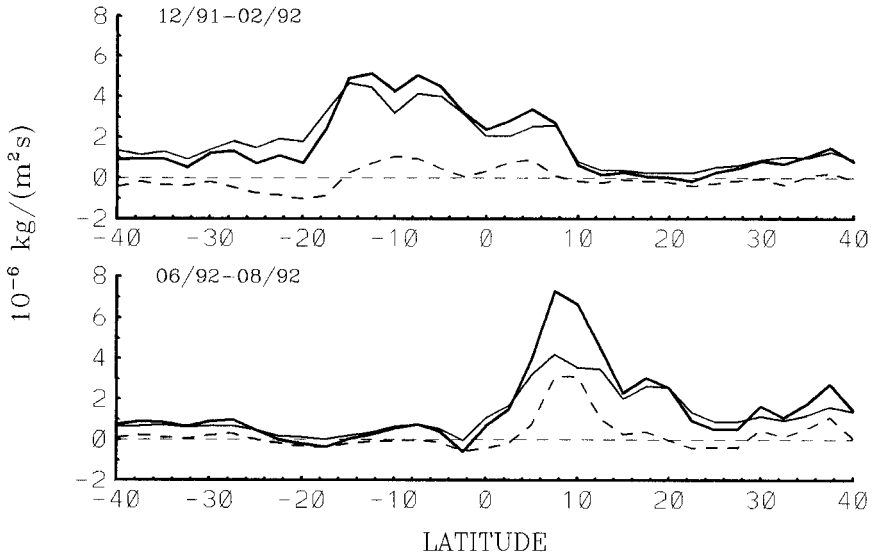

FIG. 5. Partitioned upward MLS UTH fluxes on 464 hPa; solid thin line: convective flux, dashed line: background flux. The total fluxes represented by the heavy curves are the same as in Fig. 2c.

The first half of 1992 was accompanied by El Niño over the central Pacific. The zonal mean water vapor content was slightly higher near the equator, compared with the normal year of 1994. Although there were relatively dry patches on the both sides of the warm pool in the El Niño season (Fig. 1), the moisture in the whole belts was not significantly lower than in the normal year. From June to August 1994, the upper troposphere in La Niña season was generally drier than in 1992. It should be noted that July 1994 had only 16 days of data, and June 1992 only 18 days. The dryness in the two transition seasons was also obvious in the MLS satellite data.

The annual means were slightly higher in the Northern Hemisphere than in the Southern Hemisphere for the two years. The annual mean temperatures in the lower troposphere and on the sea surface are also higher in the northern tropical and subtropical latitudes than in the corresponding southern latitudes (Peixoto and Oort 1992). So the positive correlation between UTH and SST is also a long-term mean feature. Overall, the points covered in this section suggest a positive response.

5. Dynamic processes of UTH variations

From Riehl and Malkus (1958), nearly all upward heat and mass transport in the Tropics takes place in tall cumulonimbus clouds. These convective clouds are a kind of transient perturbation, which have a lifetime shorter than that of the baroclinic cyclones at the midlatitudes. However, the vertical transient flux shown by Figs. 2c and 2d was negligibly small compared with the mean flow flux in the Tropics. So the statistics in Fig. 2 may not represent the real physical processes in the atmosphere and may not reveal the relation between deep convection and large-scale subsidence.

It was argued (Zhu and Newell 1998) that the total meridional water vapor flux in the whole atmosphere may be accomplished by four or five atmospheric rivers. Thus, the transient flux calculated with the traditional algorithm may be underestimated. Palmén and Newton (1969) pointed out that the slow mean tropical circulation should be interpreted as the statistical result of the vigorous vertical motions in convective clouds that penetrate to the upper troposphere only in a very small portion of the total region. Thus, the so-called zonal mean flow fluxes in (1) and (2) are contributed more or less by transient and local processes. This can be seen from Fig. 4, which gives the vertical fluxes of water vapor across 500 hPa over a tropospheric river, evaluated with ECMWF data at 1200 UTC 4 January 1992. A rapid developing cyclone, termed a bomb, related to this river has been discussed by Zhu and Newell (1994). Only four or five of the rivers along a typical midlatitude in the daily maps may complete the total vertical transport of water vapor at that latitude.

The *UARS* data may be used to analyze the large-scale cirrus decks in the upper troposphere and lower stratosphere. However, the large-scale cirrus may be produced by slow large-scale sloping lifting flows. Most of the cirrus that can be detected by *UARS* may not be used to indicate the local convection. The local convection will be identified in this study by the strongest vertical velocities on 464 hPa in the twice-daily ECMWF datasets, which cover 10% of the grid points at each latitude from 40°S to 40°N. This number is based on the previous work (Zhu and Newell 1998). The rest

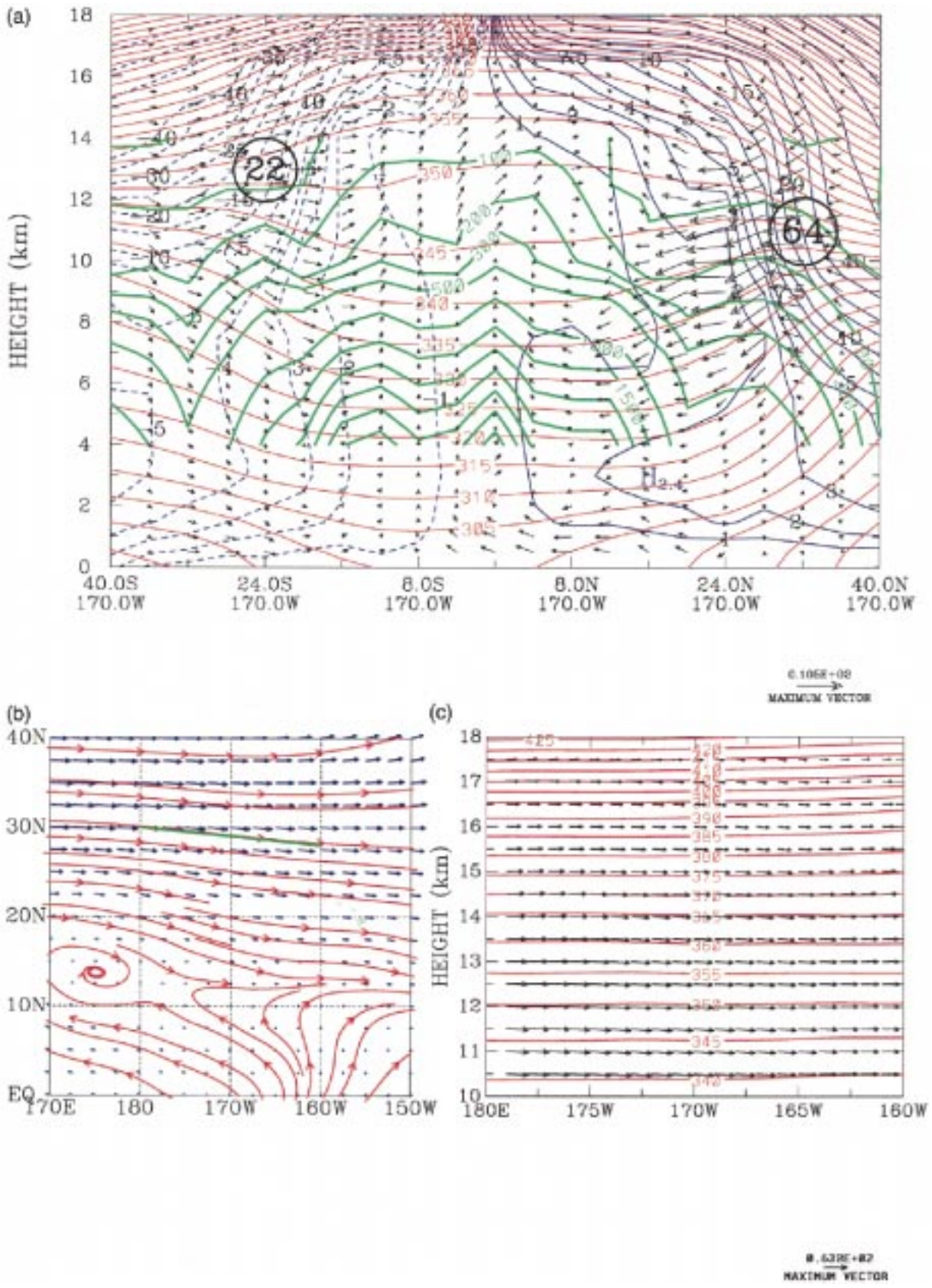
(a)
HEIGHT (km)
40.0S 170.0W
24.0S 170.0W
8.0S 170.0W
8.0N 170.0W
24.0N 170.0W
40.0N 170.0W
(b)
40N
30N
20N
10N
EQ
170E
180
170W
160W
150W
(c)
HEIGHT (km)
180E
175W
170W
165W
160W
MAXIMUM VECTOR
MAXIMUM VECTOR

is called the background flow. The vertical fluxes by the convection and background flow are displayed in Fig. 5. The ECMWF data used are in the horizontal resolution of 2.5° × 2.5°. Hence, for example, a latitude circle at 12.5°N has 144 grid points, and the 14 grid points with the largest vertical velocities are used to compute the vertical convective flux, the remaining 130 being used to compute the background flow. The local convection may happen on a smaller scale than 2.5° grids. So the convective vertical fluxes evaluated with the ECMWF data may be underestimated. The figure shows that the convective flux is stronger than the background flux. It is positive at all latitudes and accounts for the major part of total flux. The convective upward transport had a peak in the summer tropical regions, where the strongest divergence of horizontal flux took place, as shown by Fig. 2a. The downward transport was contributed by the background flows only.

The vertical influxes from the new algorithm are summarized in Table 1, which are evaluated from (4) at 464 hPa for Table 1 (upper and middle) and at 316 hPa for Table 1 (lower), assuming that the vertical fluxes across the tropopause are negligibly small. The convective flux in the tropical regions (20°S–20°N) was extremely strong in the first half of 1992 (Table 1upper), which was in an El Niño period; the induced large-scale subsidence reached the peak values in the subtropical regions. The couplings between strong convection and large-scale subsidence are indicated by the boldface numbers in the table. This approach is used to bring out the relationship between the convective upward flux and the downward flux by the background flow. Thus the tropical convection carried 424×10^6 kg s^{-1} of water vapor upward while the background flows carried 51×10^6 kg s^{-1} downward in the subtropics. In the 1992–93 period, shown in Table 1b, the pattern is essentially the same but values are much smaller in the first half of the year and somewhat larger in the second half. These facts support the hypothesis of negative response. In the normal year without El Niño (Table 1middle), strongest convection in the large area from the equator to 40°S took place in the summer hemisphere and was weaker than the southern summer convection during the 1992 El Niño period. So the induced subsidence was also weaker, with a background flux value for 40°–20°S of 39×10^6 kg s^{-1} downward for December 1991–February 1992 while this was 5×10^6 kg s^{-1} upward in December 1992–February 1993. Table 1b shows also that the convective flux in the northern subtropical region together with the induced downward fluxes on the two sides in the fall was the strongest during 1993 and was stronger than in 1992. This result is uncertain, as only eight days were available in October 1993.

The upper troposphere was not dried by the enhanced subsidence in summer as it was overwhelmed by the convective flux. Tables 2upper and 2middle give the meridional and vertical influxes of MLS water vapor into the layer from 464 to 150 hPa in 1992 and 1993, respectively. In general, the convergence of the meridional fluxes were much less than net vertical influxes into the upper troposphere. Hence the interhemispheric transport may not be critically important for the local balance of UTH. The maximum vertical flux and net influx within the latitudinal zone are denoted by the boldface numbers. The maximum influx over the tropical area from 20°S to 20°N occurred in the summer. El Niño could also have an effect on the net influx, as the influx was stronger in the first half of 1992 than in the first half of 1993. The annual mean influx in 1992 was also stronger. Comparing with Fig. 3a, we find that the high water vapor content in the summer hemisphere was related to the maximum influxes contributed mostly by local convection. That the annual mean UTH in the Northern Hemisphere was higher than in the Southern Hemisphere was also correlated to the bigger influxes.

A similar comparison of vertical influxes for 1992 appears in Table 1c for 316 to 147 hPa. The major features are the same as in Tables 1a and 1b, with absolute magnitudes of the fluxes smaller, as would be expected because both vertical air motion and humidity diminish with altitude. This table shows the same dominance of the convective flux in the water vapor across 316 hPa. The divergence of the vertical fluxes in Table 1c are compared with horizontal flux divergence in Table 2c for the 316–147-hPa layer and the 1992 year. The general pattern is similar to that in Tables 2upper or 2middle, with the vertical flux still dominating over the horizontal flux for the higher layer.

6. Slantwise convection

As discussed by Eady (1950) and Palmén and Newton (1969), the large-scale circulations at the midlatitudes may be termed slantwise convection, in which the vertical motions are a few centimeters per second compared with the horizontal wind speeds of tens of meters per second. This is also the situation for the large-scale circulation in the subtropical regions, except that the trajectory slopes in this case are larger in the meridional direction than in the zonal direction. The monthly mean

←

FIG. 6. The subtropical slantwise convection in the monthly mean ECMWF fields during Jan 1992. (a) Mean MLS UTH (green, ppmv), potential temperature (red, K), potential vorticity [blue, 10^{-7} K m^2 ($kg^{-1}s^{-1}$)], and air velocity vectors (maximum vector is 10 m s^{-1}). The interval of UTH contours is 500 ppmv over the level of 500 ppmv. The black circles indicate the subtropical westerly jets, of which the speeds (m s^{-1}) are shown at the centers. (b) Streamlines on 150 hPa. Maximum vector is 75 m s^{-1}. (c) Cross section of potential temperature (K) and air velocity (m s^{-1}) along the green line in (b). Maximum vector is 63 m s^{-1}.

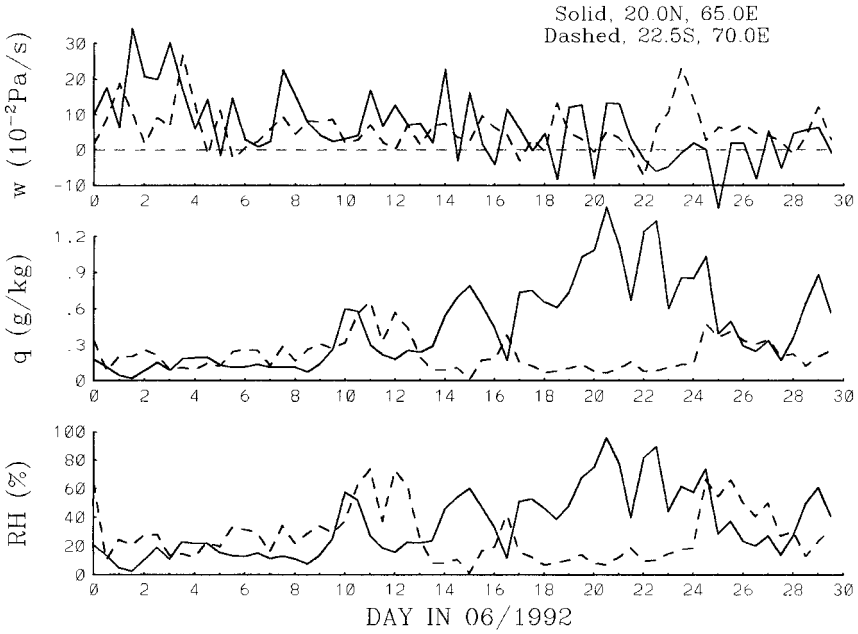

FIG. 7. Time series of ECMWF vertical velocity (10^{-2} Pa s^{-1}), specific humidity (g kg^{-1}), and relative humidity (%) on 300 hPa in Jun 1992.

winds in ECMWF data for January 1992 show a westerly subtropical jet over the North Pacific at around 32°N, with maximum speeds of 41 m s^{-1} at 500 hPa and 78 m s^{-1} at 200 hPa. These values are not the same as those shown in Fig. 6a (discussed later on), as they did not occur at the 170°W plotted in the figure. The jet in the Southern Hemisphere around 24°S was weaker. The meridional velocity of the mean circulation is also much greater than the vertical velocity. As commented upon by Green et al. (1966), the circulations of large-scale midlatitude convection may extend near the surface into much lower latitudes than is generally appreciated. Some of the local convection defined in the preceding section could be the slantwise convection in the daily fields, if the trajectory slopes were relatively small. The vertical cross sections along the trajectories of the monthly mean winds plotted from ECMWF data show that the differences between the slopes of the trajectories and isentropic surfaces are very small in the subtropical regions.

Thus, the moisture transport in the atmosphere depends not only on the vertical motions, but also on the horizontal fluxes. Figure 7 gives two examples of the local correlations between vertical motions and humidity changes, plotted from ECMWF data. The large-scale subsidence around 20°N, 65°E and 22.5°S, 70°E, respectively, induced by tropical deep convection and the Asia monsoon did not dry the upper troposphere. It is unlikely that the continuous increase of humidity over a few days was produced by evaporation of preexisting clouds. This moistening process could be contributed by horizontal transport. When the humidity surface is steeper than the isentropic surface, the large-scale downward motion on the isentropic surface may moisten the local atmosphere.

The subtropical atmosphere may be dried efficiently by the equatorward flows that come from the lower stratosphere through a folded tropopause just above and below the subtropical jets. A picture of the slantwise convection in the subtropical regions is given by Fig. 6. The maximum speeds of the descending and ascending flows in the time mean cross section was -1.9 and 2.5 cm s^{-1}, respectively. The daily values could be five times bigger over the Pacific Ocean. The adiabatic heating in the subsidence is much larger than radiation cooling. Thus, the straightforward downward motion may not be the best representation for the large-scale circulation pattern in the subtropics, except in the thermally unstable tropical atmosphere.

It is noted that the vertical and horizontal components cannot be measured directly from Fig. 6, as the vertical and horizontal scales of the cross section are different. The angles between the velocity vectors and the isentropic surfaces in the cross section may represent approximately the angles in the three-dimensional space, if the isentropic surfaces do not tilt strongly in the direction normal to the cross section. The vectors had large angles to the isentropic surfaces in the stratosphere, because the zonal tilt of the isentropic surfaces was relatively large and the flows were nearly normal to the cross section. If plotted along with the trajectories in the domains out of the Tropics, the angles become negligibly small as shown by Fig. 6c.

In general, the westerly jet cores are located in the area of tropopause folding. The equatorward flows just below the jet core may come from the stratosphere,

when they bring dry air. If we plot the temperature cross section, we may see that the tropopause was at about 8.2-km height at 40°N and 10.5-km height at 40°S along 170°W, while in the tropical regions, the tropopause is about 17 km high. Figure 6a shows that the stratospheric intrusion in the Northern Hemisphere produced a deep tongue in the MLS humidity field (~20°N, 5–9 km), together with a potential vorticity tongue below (10°–30°N, centered at 3 km). The stratospheric air may reach the tropical areas in the lower troposphere. If there is a positive correlation between increases of tropical deep convection and midlatitude baroclinic activities, the intensified stratospheric intrusion may produce a negative anomaly in the subtropical humidity field. The drying process was also evident below the southern jet (20°S, 8 km, and 32°S, 5–10 km). As a result, the equatorward horizontal gradients in the humidity field increased sharply in the subtropical upper troposphere.

The large-scale subsidence may reduce the local temperature over the sea surface when the slopes of air trajectories are less than the slopes of isentropic surfaces. At the same time, the moisture in the upper troposphere increases in the subtropical regions. So the correlation between the changes of upper-tropospheric humidity and sea surface temperature may be negative. However, it does not suggest that the response of upper-tropospheric humidity to increase in sea surface temperature over the globe is also negative. As the time mean large-scale circulations are characterized by slantwise convection, and the horizontal gradient in the humidity field is large, the effect on water vapor transport cannot be studied with a one-dimensional model.

7. Conclusions and discussion

The zonal mean MLS water vapor column content in the upper troposphere increased with increasing sea surface temperature in an annual cycle in the tropical and subtropical regions. Calculations of the fluxes with ECMWF winds and vertical velocities shows that the eddy fluxes cannot be ignored in the variations of UTH, especially in the subtropical regions. However, the traditional analyses provide little information on the dynamics of UTH variations. Using the new algorithm of Zhu and Newell (1998), we find that the increase of moisture in the upper troposphere was contributed mostly by local convection over the scattered small areas, which occupied less than 10% of the whole area, while the contribution of background fluxes and horizontal transport was relatively small.

Without using long-term climatological data, this study may not suggest an essential difference between the responses from the anomalous heating in a long-term climatology and in the seasonal cycles, since the long-term mean circulations and the interhemispheric transport do not play the most important role in the changes of UTH over the extratropical regions. It is possible that there is a limit of the positive response, over which an increase of SST will reduce UTH. However, the limitation may be caused by physical processes that are much more complicated than the large-scale subsidence.

The positive response of UTH from SST variations found here from the seasonal cycle does not nullify the existence of the negative response process suggested by Lindzen (1990). The increased tropical convection in the El Niño period enhanced the large-scale subsidence in the subtropical latitudes. The total response depends on the comparison between the positive and negative responses. Due to the local convection, the mean subsidence in the subtropical regions may not mean an overall downward transport of water vapor, even if the detrainment of clouds and evaporation in the free atmosphere are not considered. Although a positive response was suggested in the present study, the behaviors between the two hemispheres were different. Thus, a question may still remain: Does a possible manner of anomalous heating exist that will lead to an overall negative response? The model experiments of Del Genio et al. (1996) found that the response of the greenhouse effect depends largely on the change of SST gradient.

When the response from the local SST is positive, the correlation to the remote deep convection may be negative. This prevents drawing a final conclusion on the greenhouse effect in terms of the response from remote deep convection. The heating caused by greenhouse gases may not be concentrated at a particular place. A low-resolution model with simple physics may simulate the negative response but not the positive response. As convection over small areas has a great influence on the upper-tropospheric water vapor distribution, the climate model needs to be of high resolution.

Although the lower boundary is covered mostly by ocean water in the Tropics, the circulations are highly asymmetric in the zonal direction, due to the local convection. The time and zonal mean shows that the whole atmosphere in the tropical and extratropical regions rises and sinks, respectively. Although this picture fits the time-averaged energy balance equation, the mean Hadley cell may be far from the real climatology at a local place, and add little to our understanding for tropical dynamics. Using the mean circulation to replace the real circulation for the study of a nonlinear dynamic process may be misleading. For example, the time and zonal mean vertical velocities on 464 hPa evaluated by ECMWF data (figure not shown) were downward over most latitudes from 20° to 40°S in the same two seasons as in Fig. 5; simultaneously, the mean water vapor transport was generally upward.

In the physical world, the large-scale circulations in the extratropical atmosphere are characterized by slantwise circulations, as illustrated by Green et al. (1966) and shown by ECMWF data. If the adiabatic heating in a slow subsidence can be offset by radiative cooling, the cooling may take place also in the environment at a similar rate. The air motions in the diabatic process

may still have the trajectories with slopes close to or less than those of isentropic surfaces in the statically stable atmosphere. This feature remains in the time-averaged circulations. The transport in the slantwise convection has both vertical and horizontal components, and the water vapor fluxes cannot be discussed with one-dimensional models.

The drying of the subtropical atmosphere may be carried out most efficiently by the stratospheric intrusion across the humidity surfaces at midlatitudes. This process is related to baroclinic perturbations and heat balance. The relation between increases of tropical deep convection and baroclinic activity needs more study. As the Tropics get extra heating, the meridional temperature gradient and northward heat transport increase. This result may facilitate the frontogenesis and baroclinic disturbance developments in the extratropical regions. The forming of dry anomalies in the El Niño episode suggest an increase of the baroclinic activity at midlatitudes. The intensified slantwise subsidence may cool rather than heat the local atmosphere.

Acknowledgments. Support for this work came from the NASA's Earth Science Enterprise through Grant NAG 5-6710. We thank ECMWF for the use of their gridpoint data.

REFERENCES

Allam, R. J., and A. F. Tuck, 1984: Transport of water vapour in a stratosphere–troposphere general circulation model. I: Fluxes. *Quart. J. Roy. Meteor. Soc.*, **110**, 321–356.

Cess, R. D., and Coauthors, 1990: Intercomparison and interpretation of climate feedback processes in 19 atmospheric general circulation models. *J. Geophys. Res.*, **95**, 16 601–16 615.

Chiou, E. W., M. P. McCormick, and W. P. Chu, 1997: Global water vapor distributions in the stratosphere and upper troposphere derived from 5.5 years of SAGE II observations. *J. Geophys. Res.*, **102**, 19 105–19 118.

Chou, M.-D., 1994: Coolness in the tropical Pacific during an El Niño episode. *J. Climate*, **7**, 1684–1692.

Del Genio, A. D., W. Kovari Jr., and M.-S. Yao, 1994: Climatic implications of the seasonal variation of upper troposphere water vapor. *Geophys. Res. Lett.*, **21**, 2701–2704.

——, M.-S. Yao, W. Kovari Jr., and K. K.-W. Lo, 1996: A prognostic cloud water parameterization for global climate models. *J. Climate*, **9**, 270–304.

Eady, E. T., 1950: The cause of the general circulation of the atmosphere. *Centen. Proc. Roy. Meteor. Soc.*, 156–172.

Fu, R., R. E. Dickinson, and B. Newkirk, 1997: Response of the upper tropospheric humidity and moisture transport to change of tropical convection. A comparison between observations and a GCM over an ENSO cycle. *Geophys. Res. Lett.*, **24**, 2371–2374.

Green, J. S. A., F. H. Ludlam, and J. F. R. McIlveen, 1966: Isentropic relative-flow analysis and the parcel theory. *Quart. J. Roy. Meteor. Soc.*, **92**, 210–219.

Lindzen, R. S., 1990: Some coolness concerning global warming. *Bull. Amer. Meteor. Soc.*, **71**, 288–299.

Newell, R. E., Y. Zhu, E. V. Browell, W. G. Read, and J. W. Waters, 1996: The Walker circulation and tropical upper tropospheric water vapor. *J. Geophys. Res.*, **101**, 1961–1974.

——, ——, W. G. Read, and J. W. Waters, 1997: Relationship between tropical upper tropospheric moisture and eastern tropical Pacific sea surface temperature at seasonal and interannual time scales. *Geophys. Res. Lett.*, **24**, 25–28.

Palmén, E., and C. W. Newton, 1969: *Atmospheric Circulation Systems.* Academic Press, 603 pp.

Peixoto, J. P., and A. H. Oort, 1992: *Physics of Climate.* American Institute of Physics, 520 pp.

Rasmusson, E. M., 1972: Seasonal variations of tropical humidity parameters. *The General Circulation of the Tropical Atmosphere*, R. E. Newell et al., Eds., Vol. 1, The MIT Press, 258 pp.

Raval, A., and V. Ramanathan, 1989: Observational determination of the greenhouse effect. *Nature*, **342**, 758–761.

Read, W. G., J. W. Waters, D. A. Flower, L. Froidevaux, R. F. Jarnot, D. L. Hartmann, R. S. Harwood, and R. B. Rood, 1995: Upper troposphere water vapor from UARS MLS. *Bull. Amer. Meteor. Soc.*, **76**, 2381–2389.

Riehl, H., and J. S. Malkus, 1958: On the heat balance in the equatorial trough zone. *Geophysica*, **6**, 503–537.

Rind, D., E. W. Chiou, W. Chu, J. Larsen, S. Oltmans, J. Lerner, M. P. McCormick, and L. McMaster, 1990: Positive water vapour feedback in climate models confirmed by satellite data. *Nature*, **349**, 500–503.

Sandor, B. J., W. G. Read, J. W. Waters, and K. H. Rosenlof, 1998: Seasonal behavior of tropical to mid-latitude upper tropospheric water vapor from UARS MLS. *J. Geophys. Res.*, **103**, 25 935–25 947.

Soden, B. J., and R. Fu, 1995: A satellite analysis of deep convection, upper-tropospheric humidity, and the greenhouse effect. *J. Climate*, **8**, 2333–2351.

Sun, D.-Z., and R. S. Lindzen, 1993: Distribution of tropical tropospheric water vapor. *J. Atmos. Sci.*, **50**, 1643–1660.

Zhu, Y., and R. E. Newell, 1994: Atmospheric rivers and bombs. *Geophys. Res. Lett.*, **21**, 1999–2002.

——, and ——, 1998: A proposed algorithm for moisture fluxes from atmospheric rivers. *Mon. Wea. Rev.*, **126**, 725–735.